Core-Orthogonalization Effects on the Momentum Density Distribution and the Compton profile of Valence Electrons in Semiconductors

Bull. Coll. Med. Sci. Tohoku Univ. 4 (2): 93～104, 1995

Core-Orthogonalization Effects on the Momentum Density Distribution and the Compton profile of Valence Electrons in Semiconductors

Teiji KOBAYASI, Hisashi NARA*, David N. TIMMS**
and Malcolm J. COOPER***

General Education, College of Medical Sciences, Tohoku University
** Education Centre for Information Processing, Tohoku University*
*** Department of Applied Physics and Physical Electronics, University of Portsmouth, United Kingdom*
**** Department of Physics, University of Warwick, United Kingdom*

半導体の価電子運動量密度分布およびコンプトンプロファイルに対する内殻電子直交化の効果

小林悌二, 奈良　久*, D.N. ティムズ**
M.J. クーパー***

東北大学医療技術短期大学部　一般教育
* 東北大学情報処理教育センター
** ポーツマス大学 応用物理・電子工学科 (連合王国)
*** ウォーリック大学 物理学科 (連合王国)

Key words: Momentum density, Compton profile, Core-orthogonalization, Pseudopotential theory, Semiconductor

The theoretical valence electron momentum density distribution $\rho(\boldsymbol{q})$ and the Compton profile $J_z(q_z)$ of semiconductors have been studied by the pseudopotential method with a full inclusion of the core-orthogonalization (CO) in valence electron states. Since the CO introduces momentum components spreading over high momentum region, it is expected to improve usual calculation of ρ^{pseudo} and J_z^{pseudo} based on the pseudo-electron model.

Calculations are performed by the Fourier inversion formalism combined with the cubic harmonics expansion technique. Germanium is chosen as a prototype material with many core states. Results show that the CO contributions to the two quantities, $\Delta\rho$ and ΔJ_z, are fairly anisotropic. The CO contribution to the Compton profile gives J_z/J_z^{pseudo} of 0.97 at the momentum $\boldsymbol{q}=0$ with -3.3% reduction. In higher momentum region beyond the Jones zone, absolute contribution ΔJ_z is small but J_z is enhanced by 1.9～3.5 times than J_z^{pseudo} at the ΔJ_z-peak position of $q\sim1.5$ a.u.$^{-1}$, depending on the direction of observation.

§ 1 Introduction

The γ-ray Compton scattering is a powerful tool for investigating electronic structure of solids in electron momentum space[1)2)]. On the assumption of the impulse approximation, the differential scattering cross section in the independent electron model is proportional to the Compton profile J_z[3)]. The observable function $J_z(q_z)$ of the electron momentum component q_z in the direction of momentum transferred from the photon to the electron is given by the two-dimensional integration of the electron momentum density (EMD) distribution $\rho(\boldsymbol{q})$ on q_x and q_y.

For metals, the Compton profile is used as one of fundamental probes for studying the shape of Fermi surface[1)4)]. For semiconductors, the so-called Jones zone[5)] surface corresponds to the Fermi surface for metal. The volume surrounded by the Jones zone surface in the crystal wave-vector space is perfectly occupied by the valence electrons. Being different from the case of Fermi surface, the geometrical shape of the Jones zone is strictly determined by the crystallographic symmetry. If the valence electrons are hypothetically free-electron-like with no potential effect, the Compton profile should show a momentum distribution only within the momentum region surrounded by the Jones zone surface. The valence electrons in real semiconductors are fully affected by crystal potential field and, therefore, their electron states are not free-electron-like but, in general, of covalent character or of covalent-ionic mixed character in their electronic bonds. Due to the wide range of momentum spectrum introduced into the electron states as the potential effect, the momentum distribution is modified from the zeroth-order distribution mentioned above. The boundary of the occupied zone is smeared from the Jones zone and embedded in real complex momentum distribution. These deviations in the momentum distribution and then in the Compton profile are basic data for studying in detail the electronic bonding characters of semiconductors.

We have been interested in the systematic study of a series of elemental (IV) and compound (III-V and II-VI) semiconductors on their electronic bonding characters in relation to the Compton profiles and then to the momentum density distributions, within a framework of the pseudopotential (PP) theory for the electron states[6)~10)].

As discussed in detail in previous papers[9)11)~14)], in the pseudopotential theory for discussing electronic structures in the momentum space, it is important to treat the effect of the core-orthogonalization (CO) parts of the electron wave functions quantitatively. In the PP theory, the wave function of valence electron is composed of two parts ; the main part is the pseudo-wave function describing a relatively smooth-varying behaviour of the electron. The second part describes the spatially rapid oscillation of the valence electron in the inner core region, reflecting the fact that the valence electron state should be orthogonal to the core electron states.

Corresponding to the spatially rapid oscillation of this CO part, the valence electron wave functions have high momentum components, additionally to the momentum components introduced as the potential effect through the pseudo-wave functions. Coupling between the pseudo- and the CO-parts of the wave functions, therefore, affects the EMD distribution and the Compton profile over a wide range of momentum.

The purpose of this paper is to study the CO

effects on the EMD distribution and the Compton profile quantitatively, choosing Ge as a prototype semiconductor with many inner core electron states from $1s$ to $3d$. In order to keep a high accuracy in a fine mesh calculation in the space of momentum $\boldsymbol{q}$, we employ the Fourier inversion method[2)4)6)12)15)16)], or the $B(\boldsymbol{r})$-function formalism, combined with the cubic harmonics expansion technique[4)10)13)] for the function $B(\boldsymbol{r})$. Here the spatial function $B(\boldsymbol{r})$ is defined[16)] as a Fourier inversion transform of $\rho(\boldsymbol{q})$ and is calculated by using the PP wave functions. The $\rho(\boldsymbol{q})$ is obtained by Fourier-tranforming $B(\boldsymbol{r})$ and then used for calculating $J_z(q_z)$. The CO contribution to the EMD distribution, $\Delta\rho(\boldsymbol{q})$, is defined by the difference between $\rho(\boldsymbol{q})$ of the "true" valence electron system with the CO parts fully taken into account and $\rho^{\text{pseudo}}(\boldsymbol{q})$ of the pseudo-valence electron system. The CO contribution to the Compton profile $\Delta J_z(q_z)$ is also defined in the same manner.

Since the method of calculations are given in detail in refs. 10, 12 and 13, descriptions of the formalism and calculational method are briefly given in § 2. In ref. 13, our formalism in the PP framework is applied to quantitative estimates of the CO effects on the electron-positron pair momentum density (EPMD) distribution and the angular correlation annihilation radiation. Results for $B(\boldsymbol{r})$, $\rho(\boldsymbol{q})$, $J(q_z)$, $\Delta\rho(\boldsymbol{q})$ and $\Delta J_z(q_z)$ are given in § 3. The results of $\Delta\rho(\boldsymbol{q})$ and $\Delta J_z(q_z)$ are discussed in § 4.

§ 2 Brief Descriptions of Formalism and Calculations

2-1. Formalism[10)12)13)]

The basic quantity to be calculated is the EMD given by

$$\rho(\boldsymbol{q})=2\sum_{n}\sum_{k}\left|\int\Psi_{nk}(\boldsymbol{r})\exp(-i\boldsymbol{q}\cdot\boldsymbol{r})d^3\boldsymbol{r}\right|^2, \tag{1}$$

where Ψ_{nk} is the wave function of an electron with wave vector $\boldsymbol{k}$ in the nth occupied valence band. The spatial function $B(\boldsymbol{r})$ is defined by the Fourier inversion of the EMD as

$$B(\boldsymbol{r})=\sum_{q}\rho(\boldsymbol{q})\exp(i\boldsymbol{q}\cdot\boldsymbol{r})/N\Omega_0, \tag{2}$$

where $N\Omega_0$ is the volume of the crystal with N unit cells of volume Ω_0.

Let us expand $\Psi_{nk}(\boldsymbol{r})$ in terms of the plane waves as

$$\Psi_{nk}(\boldsymbol{r})=\sum_{G\in Q}C_{nk}(\boldsymbol{G})\exp[i(\boldsymbol{k}+\boldsymbol{G})\cdot\boldsymbol{r}]/\sqrt{N\Omega_0}, \tag{3}$$

where $\boldsymbol{G}$ is the crystal reciprocal lattice vector. The function $B(\boldsymbol{r})$ is explicitly written by using the expansion coefficients $C_{nk}(\boldsymbol{G})$ as

$$B(\boldsymbol{r})=2\sum_{n}\sum_{k}\sum_{G\in Q}|C_{nk}(\boldsymbol{G})|^2\exp[i(\boldsymbol{k}+\boldsymbol{G})\cdot\boldsymbol{r}]/N\Omega_0. \tag{4}$$

The relation between the expansion coefficients of the true- and the pseudo-valence electron wave functions, C_{nk} and C_{nk}^{pseudo} respectively, is given by

$$C_{nk}(\boldsymbol{G})=N_{nk}\Big[C_{nk}^{\text{pseudo}}(\boldsymbol{G})-\sum_{c}\sum_{G'\in P}b_{ck}(\boldsymbol{G}')b_{ck}(\boldsymbol{G})C_{nk}^{\text{pseudo}}(\boldsymbol{G}')\Big], \tag{5}$$

where $b_{ck}(\boldsymbol{q})$ is the Fourier coefficient of the cth inner core electron wave function multiplied by the crystal structure factor and N_{nk} is the renormalization constant for the set $\{C_{nk}(\boldsymbol{G})\}$. Because of the spatially rapid oscillation of the CO parts, the second term in the brackets of eq. (5), the reciprocal lattice vectors $\boldsymbol{G}$ should be taken from a very large set of vectors, Q, containing sufficiently large vectors than those

in a set for the pseudo-wave functions, P.

The functions $B(\boldsymbol{r})$ and $\rho(\boldsymbol{q})$ are expanded in terms of the crystal cubic harmonics K_l^i as

$$B(\boldsymbol{r})=\sum_{li}B_{li}(r)K_l^i(\Omega_r) \tag{6}$$

and

$$\rho(\boldsymbol{q})=\sum_{li}\rho_{li}(q)K_l^i(\Omega_q). \tag{7}$$

Once we have calculated the function $B_{li}(r)$

$$\begin{aligned}B_{li}(r)&=\int B(\boldsymbol{r})K_l^i{}^*(\Omega_r)d\Omega_r\\&=\frac{4\pi}{N\Omega_0}i^l 2\sum_n\sum_{\boldsymbol{k}}\sum_{\boldsymbol{G}\in Q}|\,C_{n\boldsymbol{k}}(\boldsymbol{G})\,|^2\\&\times j_l(|\,\boldsymbol{k}+\boldsymbol{G}\,|\,r)K_l^i{}^*(\Omega_{\boldsymbol{k}+\boldsymbol{G}}),\end{aligned} \tag{8}$$

where j_l is the spherical Bessel function, $\rho(\boldsymbol{q})$ is easily calculated in fine accuracy since

$$\rho_{li}(q)=4\pi(-i)^l\int_0^\infty B_{li}(r)j_l(qr)r^2dr. \tag{9}$$

The Compton profile $J_z(q_z)$ defined by

$$J_z(q_z)=(1/2\pi)^2\int_{-\infty}^{\infty}dq_x\int_{-\infty}^{\infty}dq_y\rho(q_x,q_y,q_z) \tag{10}$$

is transformed into

$$J_z(q_z)=2\pi\sum_{li}\gamma_{li}(q_z)K_l^i(\beta,\alpha), \tag{11}$$

where

$$\gamma_{li}(q_z)=(1/2\pi)^2\int_{|q_z|}^{\infty}\rho_{li}(q)P_l(q_z/q)qdq. \tag{12}$$

Here P_l is the Legendre's polynomial. The CO contributions $\Delta\rho(\boldsymbol{q})$ and $\Delta J_z(q_z)$ are defined by

$$\Delta\rho(\boldsymbol{q})=\rho(\boldsymbol{q})-\rho^{\text{pseudo}}(\boldsymbol{q}) \tag{13}$$

and

$$\Delta J_z(q_z)=J_z(q_z)-J_z^{\text{pseudo}}(q_z), \tag{14}$$

where $\rho^{\text{pseudo}}(\boldsymbol{q})$ and $J_z{}^{\text{pseudo}}(q_z)$ of the pseudo-valence electron system are derived from $B(\boldsymbol{r})$ of eq. (4) with $C_{n\boldsymbol{k}}^{\text{pseudo}}$ instead of $C_{n\boldsymbol{k}}$.

Both J_z and $J_z{}^{\text{pseudo}}$ obey the normalization condition

$$\begin{aligned}1/2\pi\int_{-\infty}^{\infty}dq_zJ_z(q_z)&=1/2\pi\int_{-\infty}^{\infty}dq_zJ_z^{\text{pseudo}}(q_z)\\&=B(0)=\text{uniform density of}\\&\qquad\text{valence electrons,}\end{aligned} \tag{15}$$

and then we have

$$1/2\pi\int_{-\infty}^{\infty}dq_z\,\Delta J_z(q_z)=0. \tag{16}$$

Equation (16) contrasts with the following condition for the contribution of the core-orthogonalization, $\Delta\Gamma_{//}(q_z)$, to the one-dimensional ACAR (angular correlation of annihilation radiation) in the positron annihilation[12)13)];

$$\begin{aligned}1/2\pi\int_{-\infty}^{\infty}dq_z\,\Delta\Gamma_{//}(q_z)&=[A(\boldsymbol{r})-A^{\text{pseudo}}(\boldsymbol{r})]_{r=0}\\&=\int[\rho_-(\boldsymbol{r})\rho_+(\boldsymbol{r})-\rho_-^{\text{pseudo}}(\boldsymbol{r})\rho_+^{\text{pseudo}}(\boldsymbol{r})]d^3\boldsymbol{r},\end{aligned} \tag{17}$$

where $\rho_-(\boldsymbol{r})$ and $\rho_+(\boldsymbol{r})$ are the valence electron- and the positron-densities, respectively. The function $A(\boldsymbol{r})$ and the definition of the "pseudo"- positron are described in refs. 12 and 13.

2-2. Cubic Harmonic Expansion[4)10)13)]

In the cubic harmonics expansions of $B(\boldsymbol{r})$ and $\rho(\boldsymbol{q})$, it is confirmed that the convergence in the expansions is fully attained by inclusion of $l\leqq 22$, with the first sixteen harmonics belonging to the Γ_1-representation of the O_h group. The relevant coefficients for constructing the harmonics are quoted from the Table I in ref. 17. In these expansions, the term with $l=0$ is the component of spherical symmetry. The sum over l in which the $l=0$ term is excluded describes the anisotropic behavior of $B(\boldsymbol{r})$ or $\rho(\boldsymbol{q})$.

2-3. Pseudopotential and Energy Band Calculation[13)18)19)]

As a prototype semiconductor, Ge with the inner core states of $1s, 2s, 2p, 3s, 3p$ and $3d$

symmetries is chosen. The PP used in the energy band calculation for Ge was determined previously[18)19)], which is a nonlocal 3L+NL(d) type PP of Heine-Abarenkov form. The coefficients $C_{nk}^{\text{pseudo}}(\boldsymbol{G})$ of pseudo-valence electron states are solved under this PP. The Chadi-Cohen's 10-special-point scheme[20)] is adopted for making a $\boldsymbol{k}$-mesh in the Brillouin zone. The total number of $\boldsymbol{k}$'s in the fcc Brillouin zone is 256. In the expansion of the pseudo-wave function, all plane waves with the O_h-group reciprocal lattice vectors G satisfying

$$|\boldsymbol{k}+\boldsymbol{G}|^2-|\boldsymbol{k}|^2\leq 20 \qquad (18)$$

in units of $(2\pi/a)^2$ are taken, where a is the lattice constant. The corresponding vector set P for the expansion includes the 137 reciprocal lattice vectors. The largest vectors are in the vector shell of (4, 4, 0) $(2\pi/a)$. The Roothaan-Hartree-Fock atomic wave functions by Clementi[21)] are used for the inner core wave functions. The coefficients $C_{nk}(\boldsymbol{G})$ of the true valence electron states are calculated by eq. (5). Because of the highly localized nature of the core functions, the reciprocal lattice vector set Q was forced to include all the 4621 vectors up to the very large shell of (13, 7, 7) $(2\pi/a)$.

§ 3 Results

We express behaviours of the three-dimensional functions of $B(\boldsymbol{r})$ and $\rho(\boldsymbol{q})$ of the true valence electron system by contour maps on the $(1\bar{1}0)$ plane containing the following five directions of [001], [112], [111], [221] and [110].

In Fig. 1, (a) shows the whole behaviour of $B(\boldsymbol{r})$ including the spherical component and (b) shows the anisotropic part of $B(\boldsymbol{r})$. The distance parameter r is in units of lattice constant a (=10.6772 a.u.). In Fig. 1(a), the heavy contour line shows zero and the light one is for positive value. The contuor spacing is 0.1 in unit of $1/\Omega_a$, where $\Omega_a=\Omega_0/2$ is the atomic volume of Ge. In Fig. 1(b), the heavy, middle and light lines are for positive, zero and negative values, respectively, with the spacing 0.01.

The directional variations of $B(\boldsymbol{r})$ along the [001], [112], [111], [221] and [110] directions are shown in Fig. 2, in units of $1/\Omega_a$.

In Fig. 3, (a) shows the distribution of the EMD $\rho(\boldsymbol{q})$ including the spherical component

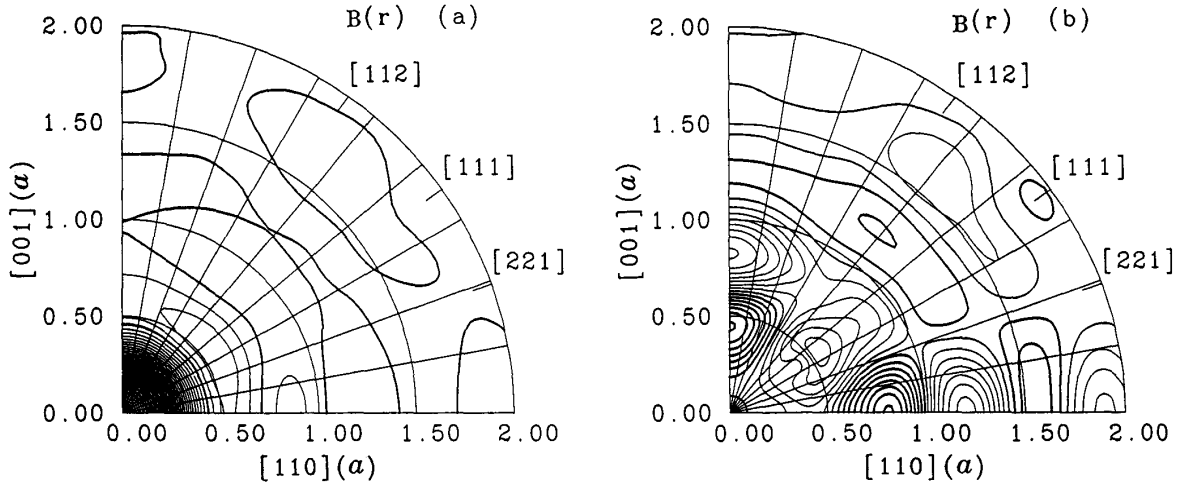

Fig. 1. Contour map of $B(\boldsymbol{r})$ of Ge on the $(1\bar{1}0)$ plane: (a) Total $B(\boldsymbol{r})$ including the spherical component. (b) Anisotropic part of $B(\boldsymbol{r})$. Types of contour lines and contour spacing in the figures are explained in the text.

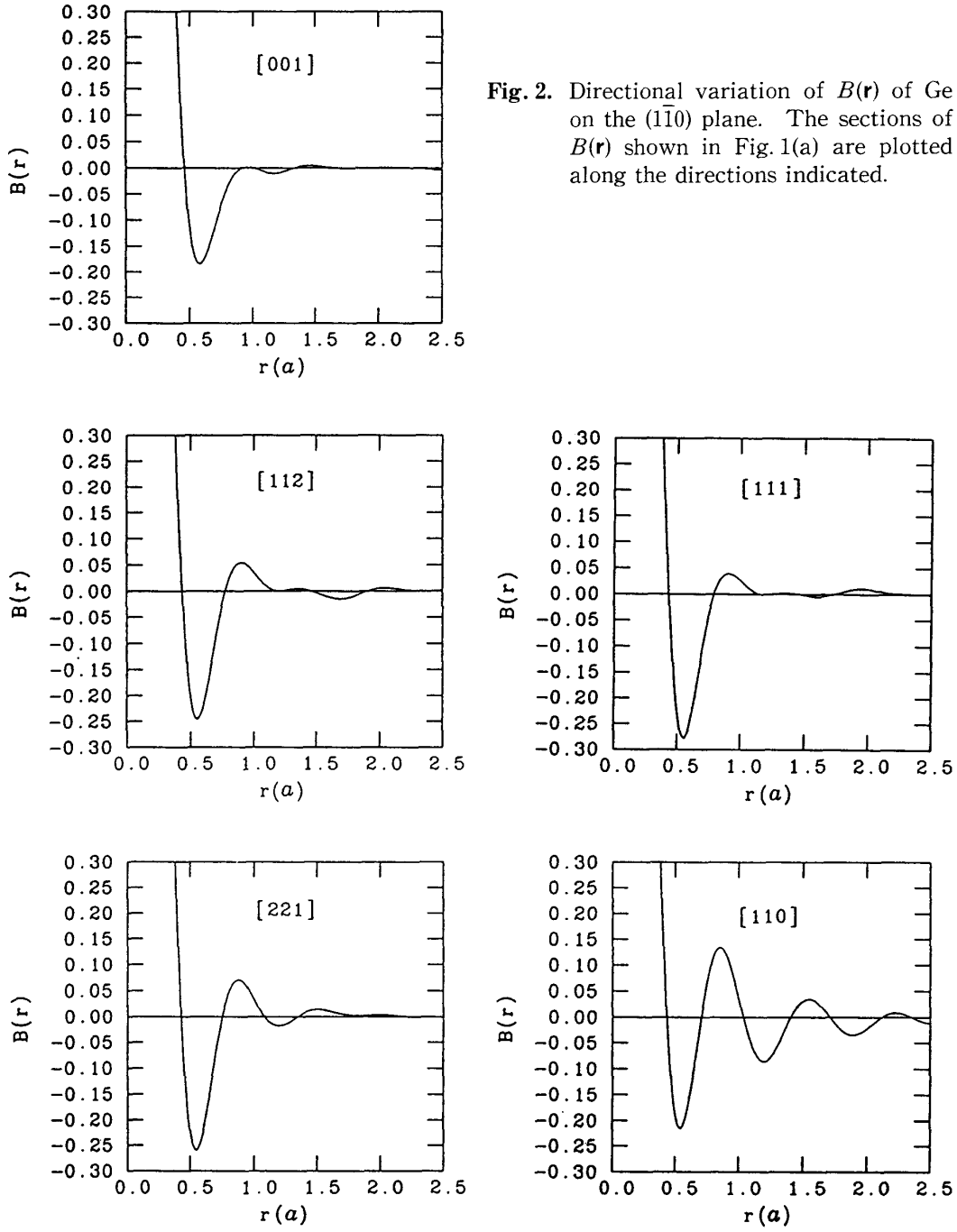

Fig. 2. Directional variation of $B(\mathbf{r})$ of Ge on the $(1\bar{1}0)$ plane. The sections of $B(\mathbf{r})$ shown in Fig. 1(a) are plotted along the directions indicated.

and (b) shows the anisotropic part of $\rho(\boldsymbol{q})$. The distance parameter q is plotted in wave-number-vector units of $(\text{a.u.})^{-1}$. In Fig. 3(a), the heavy and light lines are for zero and positive values, respectively, with the spacing 0.05 $(\text{a.u.})^3$. [In this paper $\boldsymbol{q}$ is given in units of $(\text{a.u.})^{-1}$, so that $\rho(\boldsymbol{q})$ and then $\rho_{li}(q)$ are defined to be dimensionless. By factorizing $\rho(\boldsymbol{q})$ as $\rho = (2\pi)^3 \Omega_a^{-1} \rho^c$, numerical values are given for ρ^c in units of $(\text{a.u.})^3$.] In Fig. 3(b), the heavy, middle and light lines are for positive, zero and negative values, respectively, with the spacing 0.04 $(\text{a.u.})^3$. The dashed lines inserted in Fig. 3 represent the Jones zone edge.

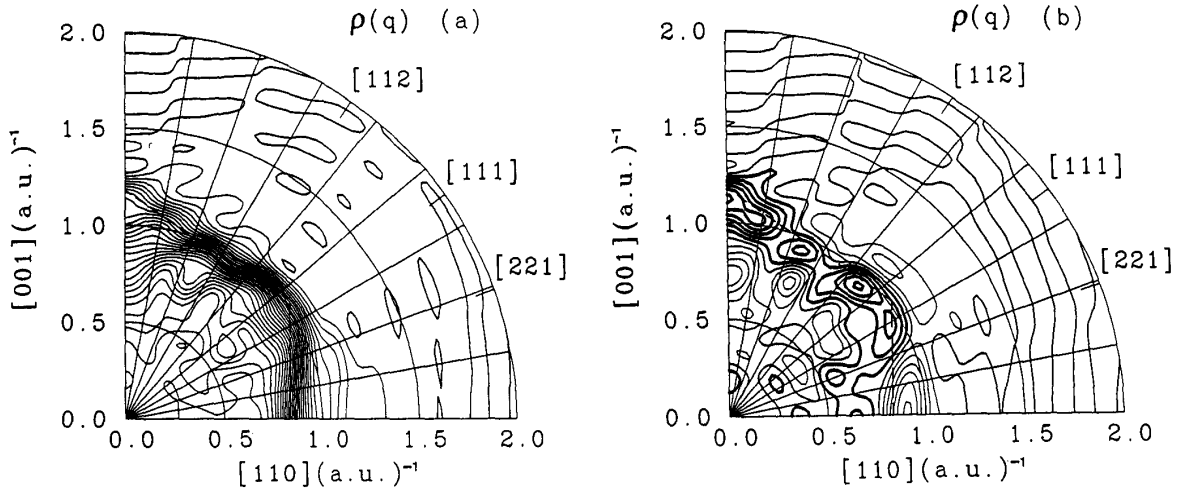

Fig. 3. Contour map of EMD $\rho(\mathbf{q})$ of Ge on the $(1\bar{1}0)$ plane: (a) Total $\rho(\mathbf{q})$ including the spherical component. (b) Anisotropic part of $\rho(\mathbf{q})$. Types of contour lines and contour spacing in the figures are explained in the text.

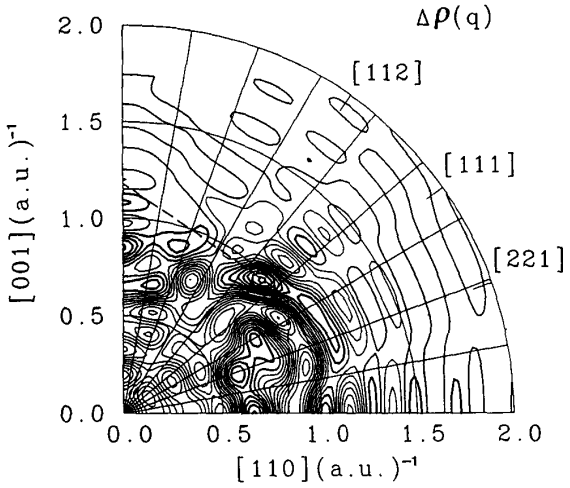

Fig. 4. Contour map of the CO contribution to the valence electron EMD, $\Delta\rho(\mathbf{q})$, of Ge on the $(1\bar{1}0)$ plane. Types of contour lines and contour spacing in the figure are explained in the text.

The pseudo-EMD $\rho^{\text{pseudo}}(\boldsymbol{q})$ of the pseudo valence electron system including no CO contribution is similarly calculated. By subtracting it from the true-EMD $\rho(\boldsymbol{q})$, the CO contribution $\Delta\rho(\boldsymbol{q})$ defined by eq.(13) is obtained. The result is shown in Fig. 4. The meaning of the contour lines is the same as in Fig. 3(b) and the contour spacing is $0.01(\text{a.u.})^3$.

The Compton profile $J_z(q_z)$ derived from the three-dimensional $\rho(\boldsymbol{q})$ are shown in Fig. 5 along the five directions given above, in a.u. [By factorizing $J_z(q_z)$ with dimension of $(\text{a.u.})^{-2}$ as $J_z=2\pi\Omega_a^{-1}J_z^c$, numerical values are given for J_z^c in a.u.] The z-components q_z of $\boldsymbol{q}$ along these directions are denoted in the figure simply as q.

The CO contribution to the Compton profile $\Delta J_z(q_z)$ of eq. (14) is obtained by using $\Delta\rho(\boldsymbol{q})$. Figure 6 shows the results of $\Delta J_z(q_z)$ along the five directions on the $(1\bar{1}0)$ plane. Note that the ordinate scale is 12.5 times larger than that in Fig. 5 for $J_z(q_z)$. Numerical values of J_z, J_z^{pseudo}, ΔJ_z and their ratios at $q_z=0$ and q_m (the peak position of ΔJ_z) are given in Table I.

§ 4 Discussions

The $B(\boldsymbol{r})$ is a function having a very large spherical component[10] around $\boldsymbol{r}=0$, similarly as the positron annihilation $A(\boldsymbol{r})$ function[13]. Figs. 1(a) and 2 show that, within the region of $r\lesssim 0.5$ (in units of lattice constant), $B(\boldsymbol{r})$ is nearly spherical. On the other hand, $B(\boldsymbol{r})$ is rather anisotropic outside the region [Figs. 1(b)

and 2].

It is noticed that, as shown in Fig. 3(a), along and near the Jones zone boundary, abrupt variations of $\rho(\boldsymbol{q})$ are pronounced. In Ge with diamond structure, there are two atoms in the unit cell. Four valence electrons are provided per atom. For full accomodation of the valence electrons in the $\boldsymbol{q}$- or $\boldsymbol{k}$-space, therefore, the Jones zone of the four-fold volume of the Brillouin zone is necessary. As is expected, the shape of the Jones zone is well caved in the $\rho(\boldsymbol{q})$ contour map of Fig. 3(a), but the deformation from the geometrically definite boundary is introduced as the potential effect; this momen-

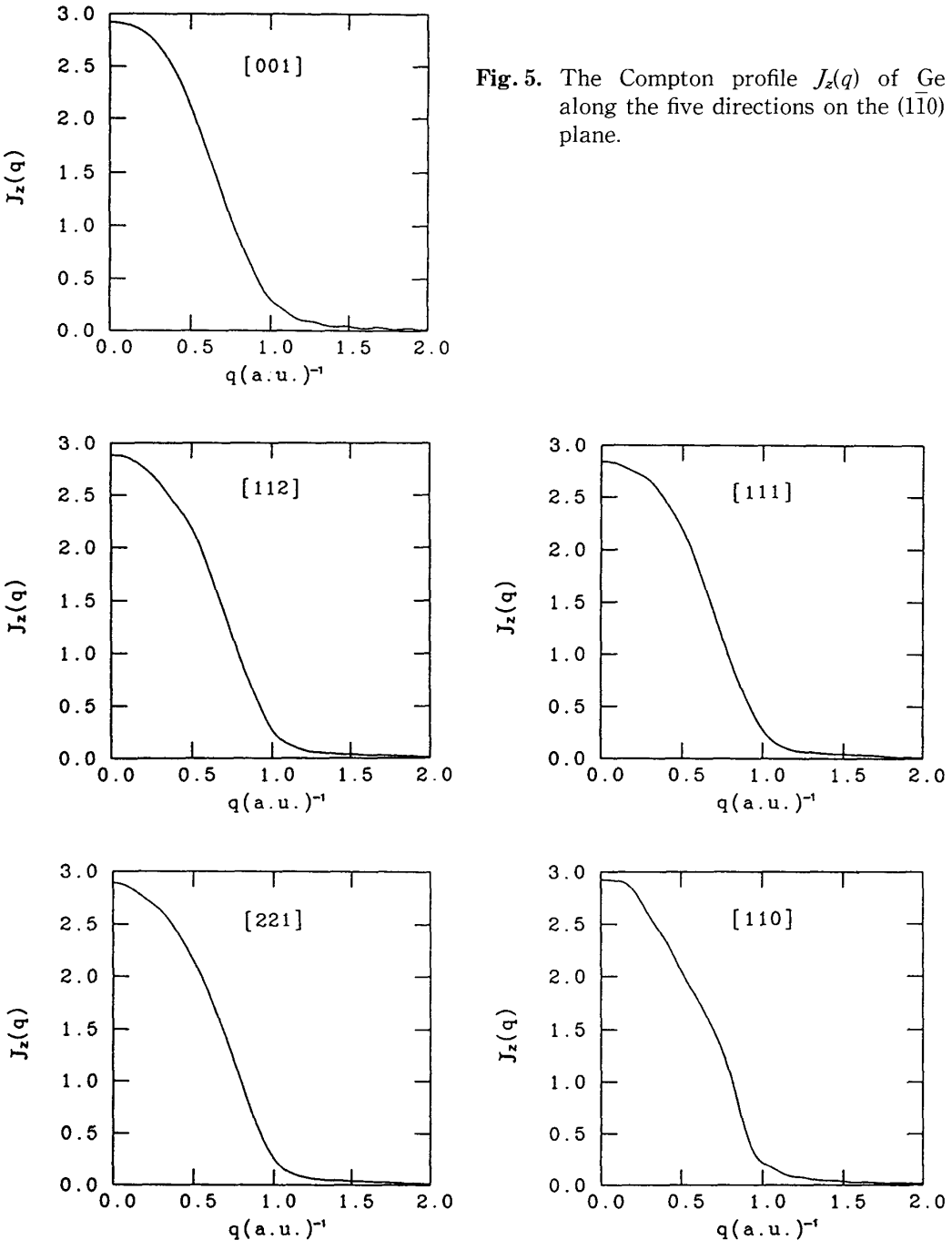

Fig. 5. The Compton profile $J_z(q)$ of Ge along the five directions on the $(1\bar{1}0)$ plane.

tum-space-effect reflects just the covalent bonding character of the valence electrons of semiconducting Ge in the real space of $\boldsymbol{r}$.

The anisotropic nature of $B(\boldsymbol{r})$ is handed over to $\rho(\boldsymbol{q})$ in the momentum space. We can observe that the contour patterns of $\rho(\boldsymbol{q})$ [Fig. 3(a)] and of its anisotropic part [Fig. 3(b)] are, as a whole, similar to those in the EPMD of Ge[13].

We can find from the results shown in Fig. 4 that the CO contribution $\Delta\rho(\boldsymbol{q})$ is not negligibly small and is clearly anisotropic.

In the high momentum region of momenta $q \gtrsim 1.5$ a.u.$^{-1}$, weak oscillating patterns of con-

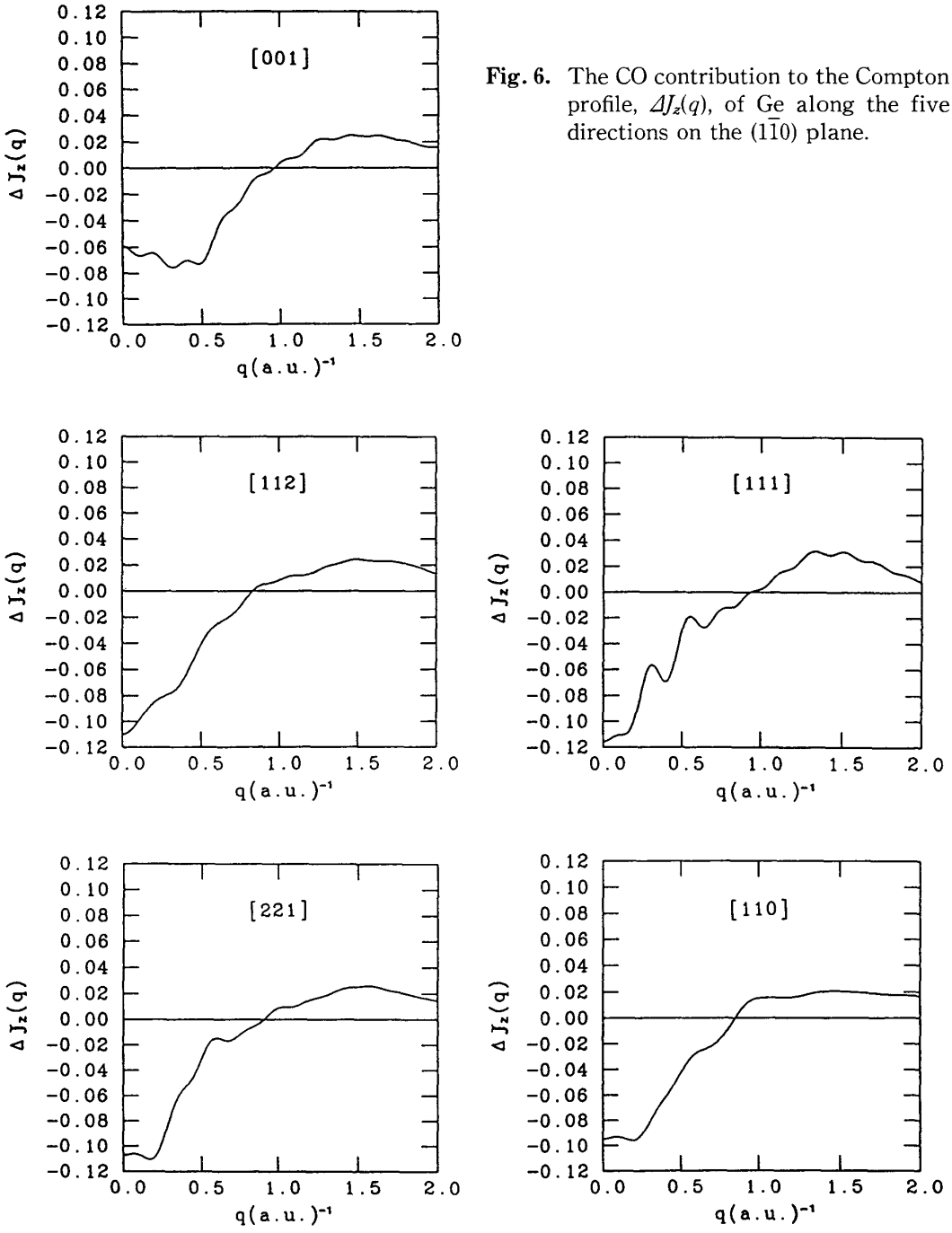

Fig. 6. The CO contribution to the Compton profile, $\Delta J_z(q)$, of Ge along the five directions on the $(1\bar{1}0)$ plane.

tour are observed in Figs. 3 and 4. These are thought to be artifactual structures introduced through the 10-point-scheme with a relatively small set of the 256 $\boldsymbol{k}$-vectors in the Brillouin zone. The next candidate is the 60-point-scheme of the 1000 $\boldsymbol{k}$-vectors[20]. In this case, a long CPU time may be necessary for the calculation under the very-high-momentum expansion of the CO parts of wave functions. Because the artifacts are not serious quantitatively, the 60-point-scheme is not tried at the present stage.

Figure 5 shows that the Compton profile $J_z(q_z)$ along any direction has a long tail beyond each Jones zone boundary. As will be shown below, higher momentum contribution to the tail region from the CO terms is fairly large. The CO contribution $\Delta J_z(q_z)$ is also ebviously anisotropic (Fig. 6), reflecting the anisotropic behaviour of $\Delta\rho(\boldsymbol{q})$. Because of the artifacts noted above, fine ripple structures remain. The $\Delta J_z(q_z)$ is negative in the lower momentum region of $q<q_0$ (q_0's are 0.97, 0.83, 0.93, 0.91 and 0.85, respectively, in the [001], [112], [111], [221] and [110] directions), and is positive in the higher momentum region of $q>q_0$. The higher momentum Fourier components in the CO parts of the electron wave functions add the positive contribution to J_z^{pseudo} and enhance it in the higher momentum region. According to eq.(15), both J_z and J_z^{pseudo} are normalized to the same value, so that the integrated value of $\Delta J_z(q_z)$ over q_z should be zero [eq.(16)]. Therefore, ΔJ_z for small q_z should be negative to compensate the positive contribution in the higher momentum region. This leads to the reduction from J_z^{pseudo} to J_z in the lower momentum region. It is in contrast with the case of the positron annihilation with eq. (17), where, as shown in Fig. 6 in ref. 13, $\Delta\Gamma_{//}(q_z)$ is positive even for small-q_z region. The results show that the relative reduction J_z/J_z^{pseudo} at $\boldsymbol{q}=0$ slightly fluctuates among the values of 0.980 ([001]), 0.963([112]), 0.961([111]), 0.964([221])

Table I. Numerical values of J_z, J_z^{pseudo}, ΔJ_z and their ratios at $q_z=0$ and q_m (the peak position of ΔJ_z). Units of Compton profiles are given in the text.

$q_z=0$					
direction	J_z	J_z^{pseudo}	ΔJ_z	J_z/J_z^{pseudo}	$\Delta J_z/J_z^{\text{pseudo}}$
[001]	2.921	2.981	−0.060	0.980	−2.01%
[112]	2.882	2.992	−0.110	0.963	−3.68%
[111]	2.843	2.959	−0.116	0.961	−3.92%
[221]	2.890	2.997	−0.107	0.964	−3.57%
[110]	2.923	3.018	−0.095	0.969	−3.15%
$q_z=q_m$					
direction	q_m (a.u.)$^{-1}$	J_z	J_z^{pseudo}	ΔJ_z	J_z/J_z^{pseudo}
[001]	1.45	0.0446	0.0196	0.0250	2.28
[112]	1.50	0.0389	0.0146	0.0243	2.66
[111]	1.51	0.0437	0.0125	0.0312	3.50
[221]	1.56	0.0369	0.0111	0.0258	3.32
[110]	1.46	0.0427	0.0220	0.0207	1.94

and 0.969([110]). The fluctuation is due to the artifacts mentioned above. The results indicate that a reasonable value of the relative reduction at $q=0$ is nearly 0.967; −3.3% reduction. On the other hand, while the absolute values of ΔJ_z in the higher momentum region are small, the relative enhancements J_z/J_z^{pseudo} are very large; as shown in Table I, they are 2.28, 2.66, 3.50, 3.32 and 1.94 at the ΔJ_z-peak positions of $q=1.45$([001]), 1.50([112]), 1.51([111]), 1.56([221]) and 1.46([110]), respectively. It is worth to note again that the CO contribution is fairly anisotropic.

It will be possible in the near future to observe experimantally the behaviour of the CO effects on the EMD distribution and on the Compton profile by high-resolutional technique in progress.

Acknowledgment

This work is a part of a research project of Studies of the Electron Distribution in Compound Semiconductors supported financially by the British Council.

References

1) Berggren, K.F., Manninen, S., Paakkari, T. *et al.*: Chap. 6 Solid, Compton Scattering, ed. by Williams, B., McGraw-Hill, New York, 1977, pp. 139-208
2) Cooper, M.J.: Compton Scattering and Electron Momentum Determination, Rep. Prog. Phys., **48**, 415-481, 1985
3) Platsman, P. and Tzoar, N.: Chap. 2 Theory, Compton Scattering, ed. by Williams, B., McGraw-Hill, New York, 1977, pp. 28-42
4) Mijnarends, P.E.: Reconstruction of Three-Dimensional Distribution, Compton Scattering, ed. by Williams, B., McGraw-Hill, New York, 1977, pp. 323-345
5) Phillips, J.C.: Pseudopotentials and Charge Densities, Bonds and Bands, Academic Press, New York, 1973, pp. 126-153
6) Nara, H., Shindo, K. and Kobayasi, T.: Pseudopotential Approach to Anisotropies of Compton-Profiles of Si and Ge, J. Phys. Soc. Jpn., **46**, 77-83, 1979
7) Nara, H., Kobayasi, T. and Shindo, K.: Anisotropies of Compton Profiles of Tetrahedrally bounded semiconductors, J. Phys. C: Solid State Phys., **17**, 3967-3974, 1984
8) Timms, D.N., Cooper, M.J., Holt, R.S. *et al.*: Compton Scattering Studies of the Valence Electron Density Distribution in GaAs, J. Phys.: Condens. Matter, **2**, 10517-10528, 1990
9) Kobayasi, T. and Nara, H.: Core-Orthogonalization Effect in Pseudopotential Theory of the Charge Density Distribution of Valence Electron in Semiconductors with Comments on the Effects in Momentum Space, Z. Naturforsch., **48a**, 193-197, 1993
10) Nara, H., Kobayasi, T., Takegahara, K. *et al.*: Optimal Number of Directions in Reconstructing 3D Momentum Densities from Compton Profiles of Semiconductors, Comp. Mat. Sci., **2**, 366-374, 1994
11) Kobayasi, T. and Nara, H.: The Valence Electronic Charge Densities of Si and Ge and the Effect of Core-Orthogonalization, Bull. Coll. Med. Sci. Tohoku Univ., **1**, 15-26, 1992
12) Kobayasi, T.: Fourier Inversion Formalism for the Calculation of Angular Correlation of Positron Annihilation Radiation of Semiconductors, Bull. Coll. Med. Sci. Tohoku Univ., **3** (1), 11-22, 1994
13) Kobayasi, T.: Core-Orthogonalization Effect on the Momentum Density Distribution of Valence Electron-Positron Pairs in Semiconductors, Bull. Coll. Med. Sci. Tohoku Univ., **4** (1), 17-28, 1995
14) Kobayasi, T. and Nara, H.: Improvement of Theoretical ACAR of Semiconductors including High Momentum Region, Positron Annihilation (Material Science Forum, Vols. **175-178**, Part. **2**), ed. by He, Y.-J., Cao, B.-S. and Jean, Y.C., Trans. Tech. Pub., Aedermannsdorf, 1995, pp. 903-908

15) Pattison, P. and Williams, B.: Fermi Surface Parameters from Fourier Analysis of Compton Profiles, Solid State Commun., **20**, 585-588, 1976
16) Mueller, F.M.: Anisotropic Momentum Densities from Compton Profiles: Silicon, Phys. Rev., **B15**, 3039-3044, 1977
17) Mueller, F.M. and Priestley, M.G.: Inversion of Cubic de Haas-van Alphen Data, with an Application to Palladium, Phys. Rev., **148**, 638-643, 1966
18) Nara, H. and Kobayasi, T.: Nonlocal Pseudopotentials of Si and Ge, J. Phys. Soc. Jpn., **41**, 1429-1430, 1976
19) Kobayasi, T. and Nara, H.: Properties of Nonlocal Pseudopotentials of Si and Ge Optimized under Full Interdependence among Potential Parameters, Bull. Coll. Med. Sci. Tohoku Univ., **2**(1), 7-16, 1993
20) Chadi, D.J. and Cohen, M.L.: Special Points in the Brillouin Zone, Phys. Rev., **B8**, 5747-5753, 1973
21) Clementi, E.: Tables of Atomic Functions, Suppl. to the paper "Ab Initio Computations in Atoms and Molecules", IBM J. Research and Develop., **9**, 2-19, 1965